Journal of Basic and Environmental Sciences

ISSN
Online: 2356-6388
Print: 2536-9202

Research Paper Open Access

Proton conducting polymeric electrolytes composed of PVA and H_3PO_4 and metal oxide

M. A. Abd Elmageed, T. Y. Elrasasi[b], R. Khalil[b]

[a] *Higher Institute For Optics Technology, Sheraton, Maser El-Gedida, Egypt.*

[b] *Physics department, Faculty of Science. Benha Univesity, Benha, Egypt.*

Abstract

Strong organic acids, such as phosphoric acid (H_3PO_4), have been trapped in a variety of polymeric solids that have been synthesised from the acid solutions. Polyvinyl alcohol (PVA)-based polymer electrolytes comprising with various concentrations of H_3PO_4 are prepared using a solution casting technique. To study conductivity and charge transport in the solid polymer electrolytes (SPEs), measurements of electrical conductivity and transference number were carried out. The frequency dependent AC conductivity at room temperature obeys the modified universal power law and the DC conductivity was obtained from the fitting parameter. The room temperature protonic conductivities of solid polymer electrolytes PVA-H_3PO_4 is higher than 10^{-4} S cm^{-1}. According to the conductivity results, the ionic conductivity of the samples increases when the amount of acid is increased. The results of the transference number measurements agree with this hypothesis. The films' temperature-dependent conductivity appears to follow the Arrhenius principle. The proton transport mechanisms are affected by acid concentrations. The characteristics of these different solid polymer electrolytes have been examined to increase the protonic conductivity and maybe apply these solid polymer electrolytes in electrochemical devices such as batteries, sensors, and electrochromic devices.

Keywords: PVA; polymer electrolyte; proton conduction

Introduction

Due to their potential use in solid electrochemical devices such as energy conversion units (like batteries/fuel cells), electrochromic display devices/smart windows, photo electrochemical solar cells, etc., ion conducting solid polymer electrolytes (SPEs) have recently gained widespread interest in the fields of solid-state electronics and Ionics[2–4]. The fundamental advantages of SPEs are their mechanical characteristics, the flexibility with which thin films of appropriate sizes may be produced, and their ability to create satisfactory electrode-electrolyte interfaces. Numerous extensively researched polymers may dissolve substantial amounts of a wide variety of salts, oxides, nanometals or acids to create SPEs [5].

Because liquid electrolytes have limitations including leakage, corrosion, and packing issues, SPEs have recently gained increased attraction with the emergence of electrochemical devices such as electrochromic and energy storage devices like batteries, supercapacitors, and fuel cells. To overcome these practical problems, SPEs or hydrogel polymer electrolytes have been employed. Therefore, polymer electrolytes such as poly (vinyl alcohol) (PVA), poly (vinyl chloride), poly (ethylene oxide) (PEO), poly (vinylidene carbonate), and poly (vinylidene fluoride) have a distinct advantage over solid electrolytes (10^{-7} to 10^{-8} $S.cm^{-1}$).

Due to their ability to produce materials with a variety of advantageous physical, chemical, thermal, and mechanical characteristics of organic and inorganic phases, inorganic-organic hybrid materials are of interest. Conductive proton in the literature, inorganic-organic hybrids with different acid species have been described [6–10].

In addition to filler additives, choosing an appropriate polymer matrix is a key to producing excellent ionic solid polymer electrolytes[11]. The fabrication of ionic solid polymer electrolytes has been described for several synthetic and natural polymers, including poly(ethylene oxide) (PEO)[12–14], cellulose[15], polyvinylidene fluoride (PVDF)[16], polyacrylonitrile (PAN)[17], chitosan [18], poly(methyl methacrylate) (PMMA)[19], starch [20], and poly(vinylidene fluoride-hexafluoropropylene] (PVDF-HFP) [21], poly(vinyl alcohol) (PVA)[22]. The synthetic water-soluble polymer polyvinyl alcohol (PVA), with excellent biocompatibility and biodegradability, as well as chemical resistance, good mechanical behaviour, adhesion, excellent film forming properties, and widespread availability, is the best candidate in the category for creating an ionic solid polymer electrolyte. As a result, considering the characteristics of the previous mentioned materials, the current study aims to develop ionic solid polymer electrolyte films of PVA using H_3PO_4 acid as the filler and investigate their suitability for use as matrix materials in ionic solid polymer electrolyte engineering applications.

Numerous researchers have examined the behaviour of acid-based polymer electrolyte complexes as proton conductors, and it has been suggested that these complexes may be used as gas sensors and electrochromic devices [23, 24].

In the conducted study, solution cast complexes of polyvinyl alcohol (PVA) with orthophosphoric acid (H_3PO_4) in thin film form have been prepared at various stoichiometric ratios. Experimental methods such as X-ray diffraction (XRD) pattern, Infra-red (IR), Scan electron microscopy (SEM), Thermal Gravimetric Analysis (TGA), Differential Scanning Calorimetry (DSC), and UV-vis spectroscopy are used to analyse thin films of PVA complexes. Wagner's polarisation and complex impedance techniques, respectively, have been used to measure electrical conductivity and transference number.

Experimental

The PVA-H_3PO_4 solid polymer electrolyte was prepared by vigorously mixing 30 mL of deionized water into 3 g of polyvinyl alcohol (PVA) at a

temperature of 95 °C. The 3 g of phosphoric acid (H_3PO_4) was added to the PVA solution after the PVA had completely dissolved, and the mixture was vigorously stirred until it had produced a homogenous, sticky solution. The mixture was then cooled to room temperature when it solidified as a clear, transparent solid polymer.

Result and discussion

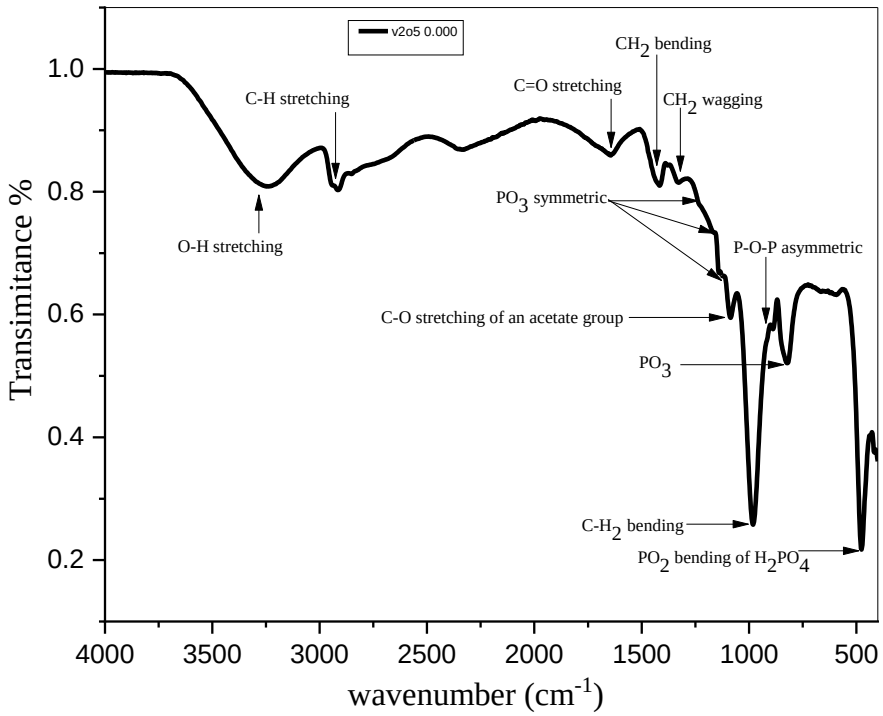

Figure 1 FTIR for PVA-H_3PO_4

The analysis of polymer structures benefits from the use of FTIR spectroscopy because it focuses on the interactions and complexation of the many components found in polymer electrolyte complexes[25]. The FTIR spectra of pure PVA and PVA complexed with various phosphoric acid concentrations are shown in Figure 1. The absorption peaks of virgin PVA are attributed to O-H stretching, C-H stretching, C-O stretching, O-H and C-H bending, and C-O stretching, respectively, at 3240, 2912, 1720, 1446, and 1096 cm^{-1}. For PVA complexed with H_3PO_4, the absorption peaks corresponding to wave numbers 3340 and 2910 cm^{-1} are discovered to be unshifted, but the peaks belonging to wave numbers 1720, 1446, and 1096 cm^{-1} are shifted to 1700, 1420, and 1085 cm^{-1}, respectively.

Additionally, for PVA complexed with H_3PO_4, all these peaks can be seen at 2325, 1329, 976, 925, 819, 584 and 476 cm^{-1} [26]. A unique interaction of the dopant with the polymer matrix is revealed by the shifting of the aforementioned wave numbers for acid doped systems compared to pure PVA, which sufficiently supports the

complexation of the system. Additionally, from pure PVA to the PVA-H_3PO_4 system, there has been a steady broadening of the peak corresponding to C-H stretching. This denotes an increase in the sample's amorphicity, which may be caused by the intermolecular forces that are random in nature and result in slightly variable force fields for each absorbing group. The examination of the DSC and XRD has revealed this sort of behaviour. However, the peak corresponding to 1720 cm^{-1} has been found to be missing in the complexed PVA in the presence of phosphoric acid. This also implies complexation and specific interaction of the dopant in the polymer matrix.

The P-O groups[27], which evolved from $(H_2PO_4)^-$ and $(VHPO_4)^{2-}$, are represented by the peaks at 986–880 cm^{-1}. While the $(VHPO_4)^{2-}$ peak changes to a lower wavenumber as the acid concentrations increase, the P-O peak can be seen emerging at 828 cm^{-1}. However, this is not the case for the $VHPO_4$ peak. The O-P-O peak for the PVA doped acid sample, however, moves to a higher wavenumber as the acid concentrations increase. It is possible to see clearly both the vibration modes in $(PO_4)^{-3}$ and the deformation of O-P-O [28].

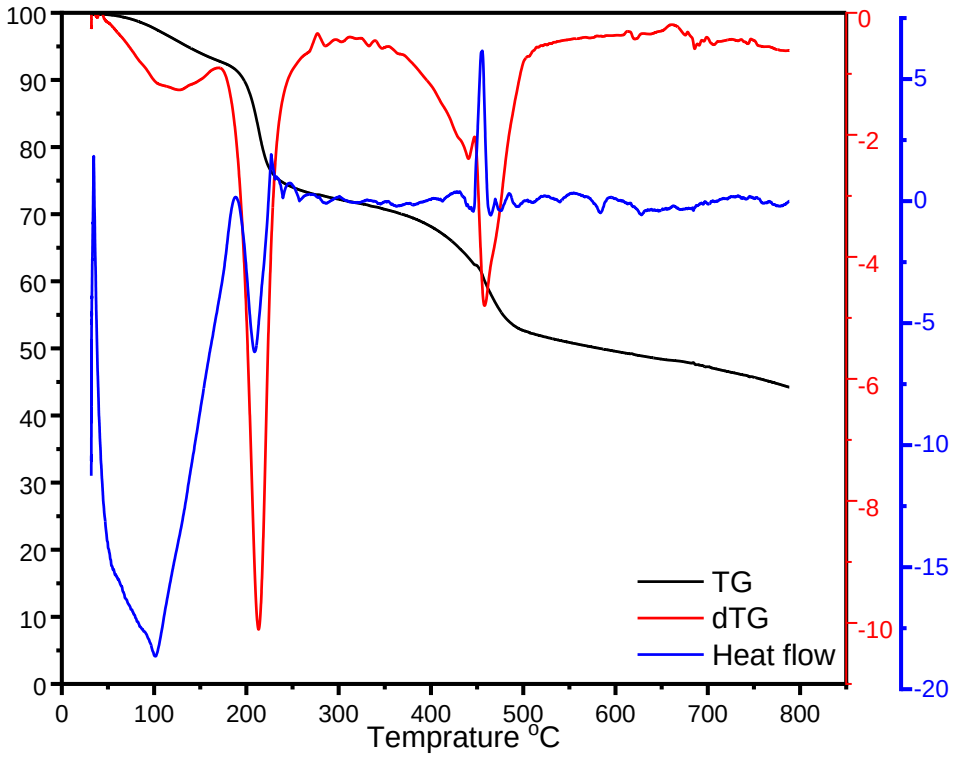

Figure 2 shows the DSC, TG and its derivative for PVA-H_3PO_4

The glass transition (T_g), melting (T_m), and crystallization temperatures (T_c) may be determined using the Differential Scanning Calorimetry (DSC) method. Figure 2 depicts the DSC thermograph for the PVA polymer film and the PVA-H_3PO_4 composite films at concentration ratios in the temperature range of 30–800 °C. In all the electrolytes, the curves exhibit a broad endothermic peak cantered at around 85 °C. This demonstrates that the overlapping between Tg transitions and any

remaining water in the electrolytes has evaporated. The melting temperature (T_m) of PVA is 240 ^oC, where an endothermic peak appears. The T_m of pure PVA powder with a hydrolysis degree of 98-99 % is approximately 225 ^oC [29]. When H_3PO_4 is doped into PVA polymer at a ratio of 1:1, it is observed that the melting temperature, Tm, of the PVA-H_3PO_4 composite polymer film shifts to a lower temperature (T_m = 213 C). With a larger concentration ratio, a lower T_m indicates a transition from a semicrystalline to an amorphous phase. The results for T_g and T_m match those from other publications [30, 31]. [Exothermic peak at 456 ^oC].

The thermal stability of PVA is an important factor in the thermal processing of PVA. TGA was used to examine the thermal stability of pure PVA and PVA-H_3PO_4 composites. From room temperature to 800 ^oC, measurements were recorded. The TGA traces were displayed in Figure 2. Water loss may be primarily responsible for the mass loss below 200 ^oC. The thermal decomposition of pure PVA begins nearly at the same temperature as T_m. The initial decomposition temperature of PVA significantly increases to a higher temperature, around 213 ^oC, with the addition of phosphoric acid. The decomposition temperature was substantially lower than T_m, which was much higher. It is evident that the phosphoric acid inclusion gave PVA its thermal processing window, or 213 ^oC. When compared to pure PVA, PVA's thermal stability increased, which indicates a strong interaction between PVA's hydroxyl groups and phosphoric acid. Previous research [32] established a two-step process for the heat degradation of PVA, which is started by the removal of side groups from the main chain. The elimination of the hydroxyl and acetate side groups is the first stage of PVA's breakdown. The percentage of acetate side groups is quite low in completely hydrolysed PVA. These show that at least hydroxyl groups are involved in the heat degradation of PVA, and that hydroxyl group stability is essential for PVA stabilization. The phosphoric acid could form strong interactions with the hydroxyl groups of PVA, and thus the thermal stability of PVA was improved. It is also likely that the endothermic nature of the melting process in plasticized PVA at about 213 ^oC would inhibit the degradation process and improve the thermal stability of PVA[33].

The TG and differential gravimetric analysis (DTG) thermographs of the PVA and PVA-H_3PO_4 composite solid polymer electrolyte are shown in Figure 2. The PVA- H_3PO_4 polymer films' TG and DTG curves showed three primary weights loss zones, which were represented by three peaks in the DTG curves. The evaporation of physically weak and chemically strong bound H_2O caused the first region, which was at a temperature of 40–170 ^oC (T_p, 1 at 115 ^oC), to form; this caused a weight loss of 6.5-8.7 wt.%. The degradation of the side chain of the PVA- H_3PO_4 solid polymer electrolyte caused the second transitional region to occur at around 170 to 270 ^oC (T_p, 2 at 213 ^oC); the overall weight loss at this stage was between 20–24 wt%.

The cleavage of the PVA-H3PO4 solid polymer electrolyte's C-C backbone, or "carbonation," caused the third stage to peak at 460 ^oC (Tp,3 at 435 ^oC), with a total weight loss of around 55 wt% at 800 ^oC.

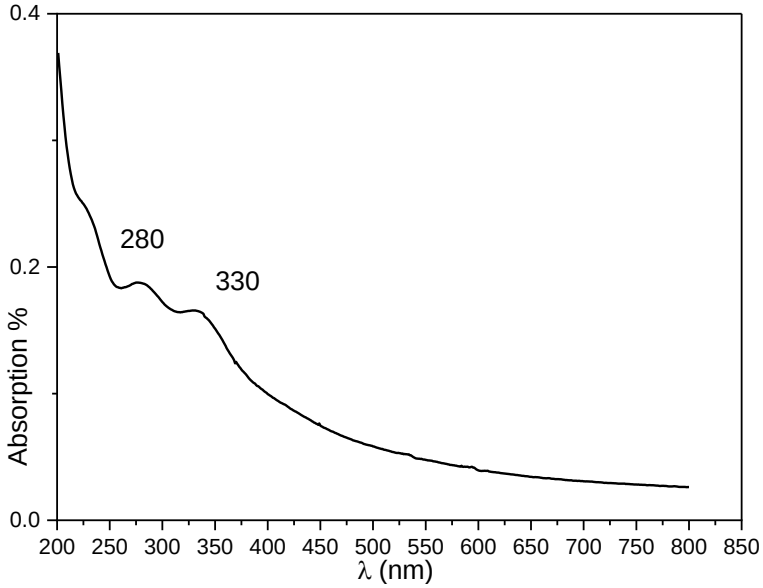

Figure 3 the Uv-vis absorption spectra for PVA/H_3PO_4

Figure 3 [34], displays the absorption spectra for films consisting of solid PVA and PVA-H_3PO_4 at mole concentration. In contrast to the reaction between PVA and H_3PO_4, which only exhibits one absorption band at 274 nm because of the interaction of PVA with the phosphate component, pure PVA has absorption bands at 204, 220, 280, and 330 nm [35]. The results of this investigation show good agreement [36]. The production of intra-and intermolecular hydrogen bonds, especially between the H_3PO_4 ions and nearby OH groups, is shown. As a result of changes in crystallinity within the polymer matrix, the bonds reflect changes in the energy band gap.

The samples were subjected to Impedance Spectroscopy (IS) experiments at different temperatures using a sinusoidal signal of 10 mV with a frequency range of 20 Hz–10 MHz. The Nyquist plot from the IS measurement on the SPE samples with 0.1, 0.2, 0.3, and 0.4 wt % of phosphoric acid is shown in Figure 4a. Since the curves in the Nyquist plot initially overlapped, they were offset on a logarithmic scale for a clearer perspective.

To get the bulk conductivity[37], σ_b, using this relation $\sigma_b = \frac{1}{R_b}\frac{t}{A}$ (1), the bulk resistance (R_b) value of the sample was determined from the Nyquist plot in the intercept of the lower frequency region on the Z' axis, where t and A are the thickness, area of the sample, respectively. The high frequency region of the Nyquist plot for the SPE samples shows a semicircle, while the low frequency region shows a spike, showing the typical behavior of a supercapacitor. The increase in acid content causes a decrease in bulk resistance and a prolongation of the spike, and the primary cause of total conductivity is ionic conduction[38].

The relationship between conductivity and the weight fraction of phosphoric acid in the solid polymer electrolytes is displayed in Figure 4b. When 0.1, 0.2, 0.3, and 0.4 wt % of phosphoric acid are added, the conductivity of the solid polymer electrolyte samples is

drastically improved by 2 orders of magnitude. The conductivity increases steadily at 0.4 wt % phosphoric acid. It is generally known that the charge (q), charge number (n), and mobility of charges (μ) have an influence on the conductivity of polymer electrolytes, and this relation can be used to explain it [39]:

$$\sigma = \sum qn\mu \quad (2)$$

Therefore, an increase in the number of charge carriers and their mobility might be responsible for the conductivity increasing with increasing acid concentration. When more than 0.3wt % phosphoric acid is introduced, the solid polymer electrolyte samples reach saturation, which reduces the amount of free space in the samples and lowers the ionic conductivity[40]. The number of charge carriers is reduced as a result, which is probably caused by the development of ion aggregates or scattered [41].

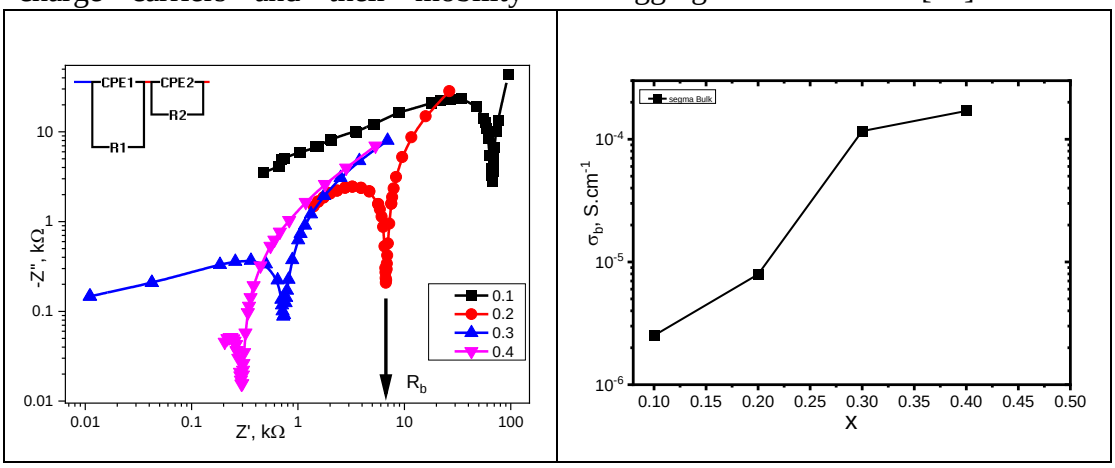

Figure 4: (a) Cole-Cole plot for PVA with different concentration of H_3PO_4, (b) Relation between concentration and σ_b

The subsequent Nyquist plots were investigated using EIS software based on the electrical equivalent circuit observed in the inset of Figure 4a. The high, middle, and low frequency regions mainly consist of the Nyquist plot's frequency range. Based on the equivalent circuit, a sample's non-zero semicircle intersects at high frequencies, which is explained (R_s). It is the result of the interaction between the polymer electrolyte resistance, the interfacial resistance at the interface of the active material and substrate, and the internal resistance of the electrode material. The obtained R_s value of 0.4 wt % PVA-H_3PO_4 solid polymer electrolyte is 130 Ω. This clearly reveals that R_s appears due to high addition of H_3PO_4 in the polymer.

The frequency dependence of ac conductivity for various concentrations of phosphoric acid in the SPE samples is shown in Figure 5a. For all SPE samples, a consistent pattern in the variation of the frequency vs ac conductivity is shown. The curves are divided into two separate regions: at lower frequencies, near 10 kHz, the ac conductivity is shown to increase with frequency, indicating the electrode polarization phenomenon [42], and at higher frequencies, from 10 kHz to 1 MHz, the frequency independent plateau region appears. The dispersion region is the third region above 1 MHz. A convenient formalism Jonscher's universal power law $\sigma(\omega) = \sigma_{dc} + A(\omega)^s$ (3) helps to explain the variation of conductivity in SPE [43,44]. The DC conductivity, σ_{dc}, includes the frequency-independent ac conductivity. The σ_{dc} of the prepared SPE samples was obtained by extrapolating the plateau region on the s-axis. The computed σ_{dc}

values from the conductivity-frequency dependency plots and those derived from the Cole-Cole plot are in good agreement with one another [45]. This study's investigation of conductivity-frequency dependency is quite comparable to earlier work that was published and focused on ionically conducting polymers, glasses, and doped crystalline solids [46,47]. The mechanism of charge transport behavior of charge carriers is supposed to match this.

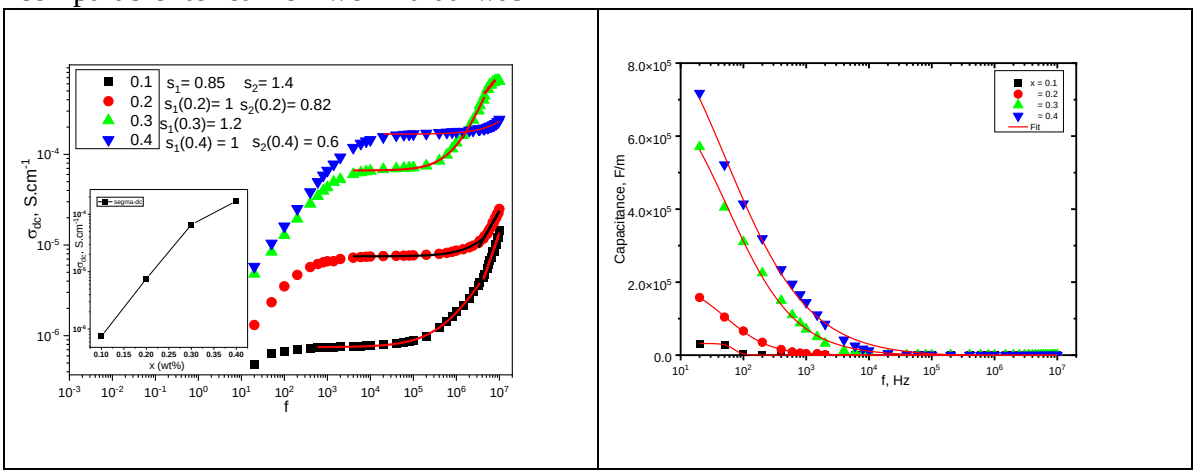

Figure5 : (a) variation of the frequency Vs ac conductivity, (b) variation of the frequency Vs Capacitance for PVA with different concentration of H_3PO_4

In addition, as the concentration of phosphoric acid increased, so did the length of the spike region in the Nyquist plot and the frequency dependence of ac conductivity at low frequencies that correspond to the capacitance of the electrode polarisation. Figure 5b displays the capacitance vs. frequency. As can be observed, the capacitance increased dramatically as the frequency decreased at the low frequency side (f ≤ 100 kHz). This increment increased as the ionic concentration level increased, indicating that a higher ionic concentration level is quite effective at increasing the capacitance. Capacitance values are more stable in the high frequency range (f > 100 kHz); all ionic solid electrolytes, glasses, and doped crystalline solid materials have identical capacitance. This is since a strongly alternating current cannot flow through accumulated ionic charges at the electrode/electrolyte interface.

With increasing frequency[48], the frequency dependent impedance (Figure 6a) decreases in both the lower and higher frequency regions. The middle frequency region's observed frequency independent impedance shows ionic transport from the electrolyte to the electrode. However, spectra show that impedance decreases in the middle frequency range as acid content increases, which may be caused by the electrolyte's increased ionic charge carriers (ionic conductivity/diffusion or frequency dependent ionic diffusion).

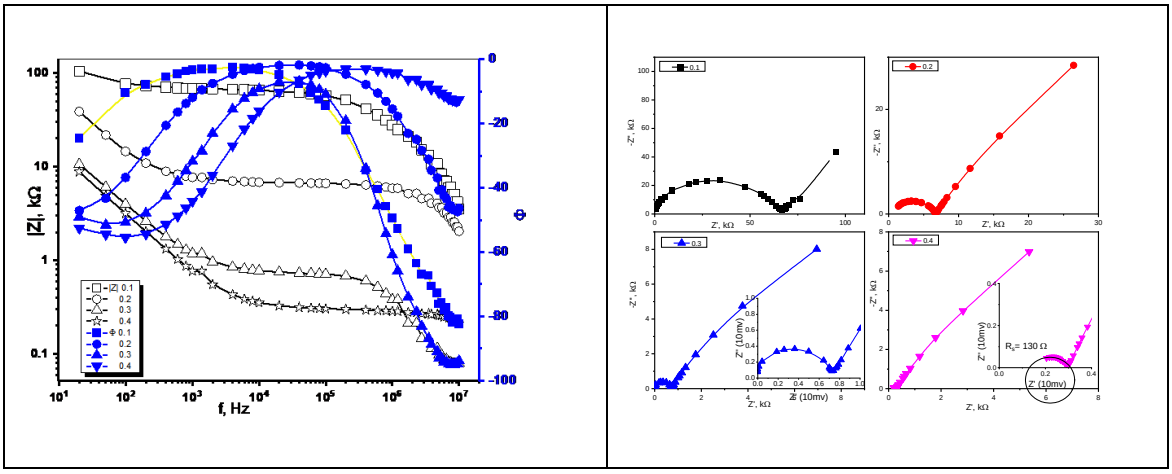

Figure6 : (a) Variation of frequency with Z and Φ, (b) Cole-Cole plot for PVA with different concentration of H_3PO_4

The ideal-capacitive character is also revealed by the higher phase angle values (Figure 6a) of-83^o and-89^o for x = 0.3 and 0.4, respectively, as it is closer to-90^o. Even though x = 0.1 and 0.2 have a low phase angle, this may be due to the partial ideal capacitive behaviour or the redox nature of the systems [49] However, the reduced phase angle causes ionic diffusion to take place [50]. According to Figure 5b, which shows a drop in capacitance as frequency increases, a significant amount of capacitance is produced at low frequencies as opposed to high frequencies.

The complex impedance plane plots (*Z*' vs *Z*'') are given in Figure 7. Usually a conduction process results in a semicircular arc in a linear complex plane plot. The log-log presentation in Figure 4a enables us to compare two responses with vastly different impedances in one plot. Despite the curved semicircular arcs, the logarithmic plot, moreover, has several positive effects, as Jonscher has noted [51].

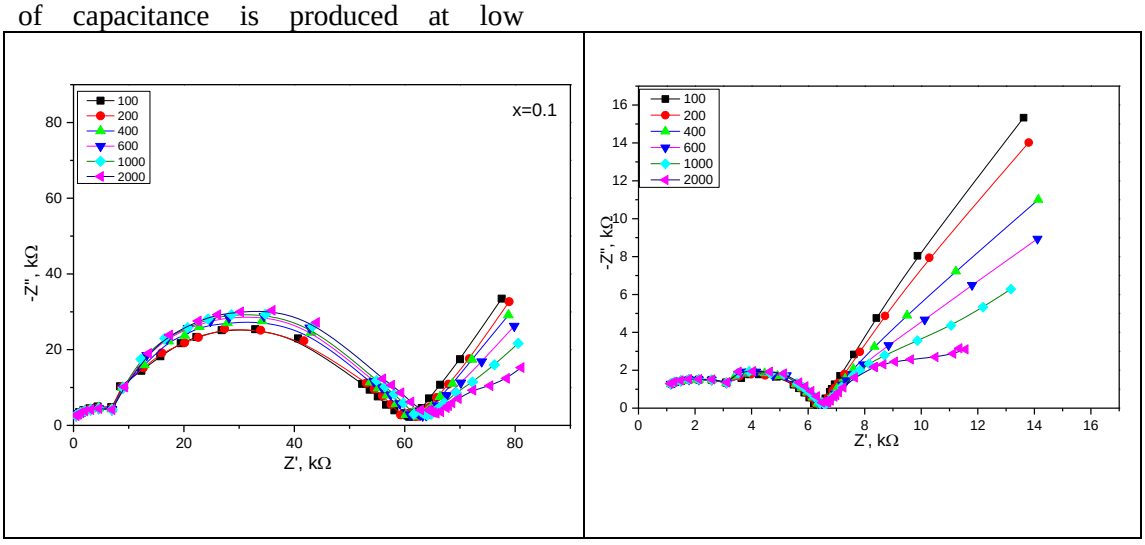

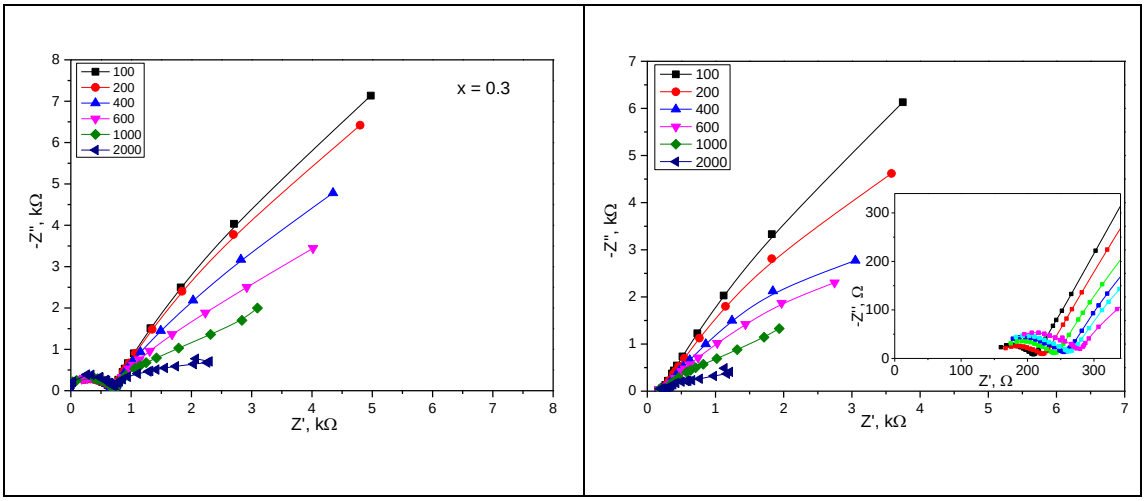

Figure 7 Cole-Cole plot for PVA-xH_3PO_4 (x= 0.1, 0.2, 0.3, and 0.4 wt%) at different frequencies

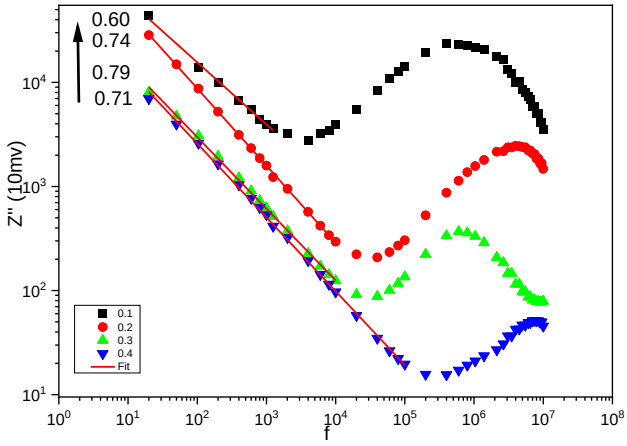

Figure 8 Relation between the frequency and the imaginary part of impedance with different concentration of H_3PO_4

In Figure 8 we present the frequency dependence of the imaginary part Z'' of the impedance $Z^* = Z' - iZ''$ at different acid concentration. We observe at x= 0.1 a higher peak at about 10^4 Hz, shifting to higher frequencies with decreased intensity as the acid concentration increases. At x = 0.4 it moves close of the frequency range of our experiment. This implies both electrical responses are thermal activated.

Dielectric studies

It is important to evaluate the dielectric relaxation to analyse the composition, physical characteristics, and electrochemical properties of solid polymer electrolytes and the composites they correspond to. Additionally, investigations of solid polymer electrolytes' dielectric and dipole relaxation over a broad frequency range are required and advantageous [52-54]. One of the effective and efficient methods for studying the mechanism of ion transport is dielectric spectroscopy [52-55]. Complex electric modulus (M*) and complex dielectric constant (ε*) measurements are required to achieve this aim. The dielectric constant (ε′) and dielectric loss (ε'') are depicted in Figure 9: (a) and (b) compared to electrolyte systems that operate at ambient temperature. The magnitudes of ε′ and ε'' utilising the formulae shown below [52-54],[56]:

$$\varepsilon' = \frac{Z''}{\omega C_o (Z'^2 + Z''^2)} \quad (4)$$

$$\varepsilon'' = \frac{Z'}{\omega C_o (Z'^2 + Z''^2)} \quad (5)$$

Where $C_o = \varepsilon_o A/d$, ε_o is the free space permittivity (8.854×10^{12} F m^{-1}) and is the angular frequency. In contrast, it is nearly a plateau at a higher frequency. The value of ε′ and ε" is very large inside the low-frequency range. It's interesting to note that at low frequencies, electrode polarisation causes charge build-up from free mobile ions at the electrode-electrolyte interfacial region, resulting in a thin layer of capacitance [57-58]. The applied electric field, on the other hand, quickly restores, and the majority of the ions may continue to exist in the majority of the sample. As a result, the electrode polarisation is reduced, which lowers the values of ε' and ε" [52-54],[59].

It is observed that the ε' increases as the acid content increases. This is because there are more charge carriers, which results in more polarisation [60-63]. These results indicate that the dielectric constant may be used to easily control the conductivity of polymer electrolytes. The mathematical formula $n_i = n_o \exp(U/\varepsilon' K_B T)$ (6), where U is the energy of dissociation, has already been used to demonstrate the significant correlation between and the density of charge carriers (n_i) [52,54,62-63]. In other words, a reduction in causes a reduction in DC conductivity. Two polymer factors that govern the DC ionic conductivity of polymer ion-conducting electrolytes are the density of charge carriers (n_i) and their mobility (μ_i) ($\sigma = \sum q n_i \mu_i$), where q is the charge on the ion carriers [52,54]. A precise study of ε′ is useful in that one can achieve a complete understanding of the electrical properties of polymer electrolytes, particularly the conductivity.

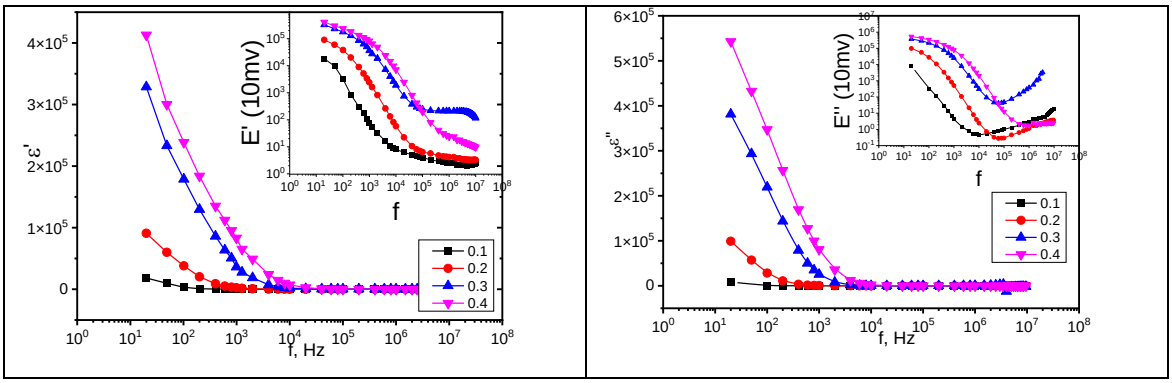

Figure9 (a) Dielectric constant and (b) dielectric loss versus log (f) for PVA-xH_3PO_4 (x= 0.1, 0.2, 0.3, and 0.4 wt %)

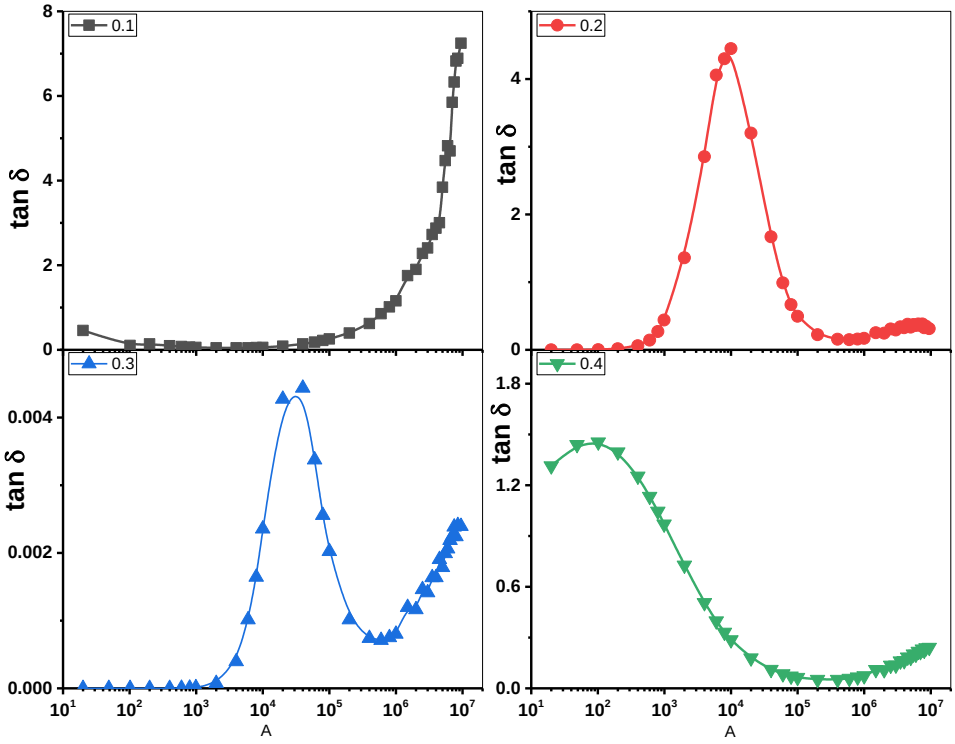

Figure 10 Tan δ versus log (f) for PVA-xH_3PO_4 (x= 0.1, 0.2, 0.3, and 0.4 wt %)

This formula, Z* = R - jX_C (7), where R and X_C are the resistor element and the capacitive element, respectively, mathematically defines the complex impedance function [63]. According to the impedance's above mathematical function, a significant amount of current flows through the resistor element at low frequencies because the capacitive component is prominent. It is noticed that from the tan δ = ε”/ε’ (8) relationship, the tan δ is directly proportional to ε”.

There are two types of dipoles that can create peaks in highly electrically conductive polymer electrolyte systems: induced and permanent. The low-frequency relaxation peaks may disappear as a result of these dipoles being hidden by the polarisation relaxation of mobile charged species that are present in the material [64-65]. The dielectric loss tangent (tan δ) versus frequency is shown in Figure 10 and can be used to understand the relaxation process. Koop’s phenomenological model is used in the interpretation of the shape of tan δ [63,66]. The model's guiding principles state that tan δ increases with increasing frequency until it reaches a maximum value, at which point it begins to decrease. The explanation is since the Ohmic component of the generated current grows noticeably relative to its capacitive component in a low-frequency region where tan δ increases. In contrast, the Ohmic component is essentially frequency independent in the high-frequency region, where tan δ drops and the capacitive component grows, resulting in a modest value of capacitive reactance[63,66-67]. Additionally, the wide nature of the tan δ peaks[68-69] is proof of the relaxation process' non-Debye type behaviour.

One can study the dielectric response that results from ion relaxation in which the electrode polarisation effects can be suppressed; in other words, small features in the high-frequency region are

recognised[70]. Through the equations shown below[71-72], the impedance data correlate the real and imaginary parts of the electric modulus.

$$M' = \frac{\varepsilon'}{\varepsilon'^2 + \varepsilon''^2} \quad (9)$$

$$M'' = \frac{\varepsilon''}{\varepsilon'^2 + \varepsilon''^2} \quad (10)$$

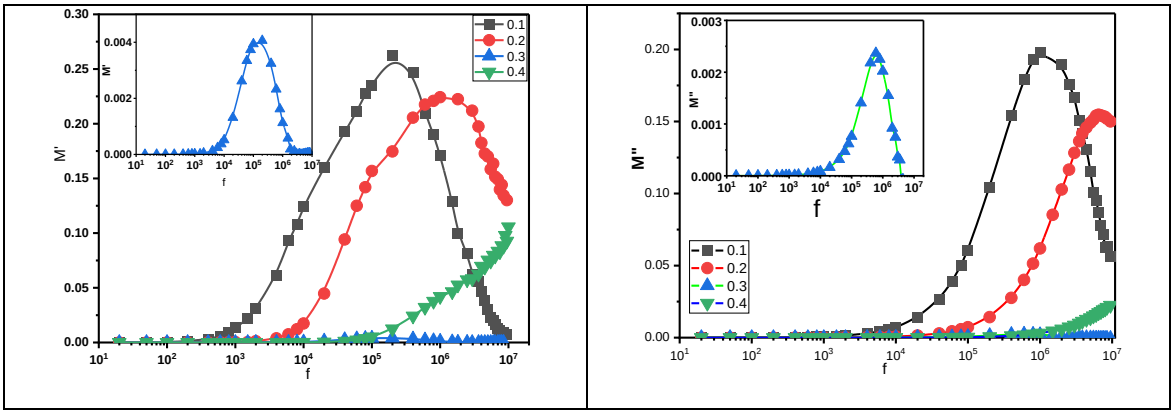

Figure11 the electric modulus versus log (f) for PVA-xH_3PO_4 (x= 0.1, 0.2, 0.3, and 0.4 wt %) (a) Real component and (b) imaginary component.

Figure 11: (a) and (b) shows that the real and imaginary components of the electrical modulus plot, which correspond to M′ and M", are frequency dependent. The low-frequency region is where the data points for the real component of the modulus spectra are situated. This could be caused by the electrodes' high capacitance, which helps the ion conduction process' migration. It can be shown that in the high-frequency range, M′ approaches its maximum saturation level. The ε′ decreases to a minimum, whereas M′ increases to a maximum ($M_\infty = 1/\varepsilon_\infty$) [73]. The samples are non-Debye because the frequency increases cause dispersion in M′ [74]. Figure 11b displays the imaginary component of the modulus spectra. It is seen that; the conductivity relaxation peaks appear at low phosphoric acid concentration. It also is notable that there is decrease of peak and a shift of peak position to the higher frequency region with the addition of further acid concentration.

In addition, the translational ion dynamics and conductivity relaxation of the mobile ions are likely to be connected to some of the peaks in the M" spectra. The segmental mobility of the polymeric chain reduces the relaxation time and accelerates ion transport during the amorphous phase. To be accurate, the ionic charge carriers' relaxation time τ is indicated by the mathematical relationship $\tau = 1/2\pi f_{max}$ [75]. The relaxation peaks are shown to have shifted to the lower frequency side in Figure 11b. This is because the presence of phosphoric acid increases ionic conductivity, which reduces the relaxation time.

Conclusion

In this study, we have introduced the noble of the pure solid polymer electrolyte at room temperature used as an electrolyte as well as a separator from the piece of PVA and H_3PO_4 such that, the PVA samples were kept constant while the phosphoric acid was varied at 0.1, 0.2, 0.3 and 0.4. the PSPE results in higher conductivity of $2x10^{-4}$ Scm^{-1} at the compositions of 0.4, in addition to that, we also observed that, the bulk modulus R_b decreases with increasing concentration, recording 100 Ω at the highest compositions of 0.4.

References

[1] G. K. Prajapati and P. N. Gupta, "Nuclear Instruments and Methods in Physics Research B Conduction mechanism in un-irradiated and c -irradiated PVA – H 3 PO 4 polymer electrolytes," *Nucl. Inst. Methods Phys. Res. B*, vol. 267, no. 19, pp. 3328–3332, 2009, doi: 10.1016/j.nimb.2009.07.006.

[2] S. B. Aziz *et al.*, "Impedance, circuit simulation, transport properties and energy storage behavior of plasticized lithium ion conducting chitosan based polymer electrolytes," *Polym. Test.*, vol. 101, no. December 2020, p. 107286, 2021, doi: 10.1016/j.polymertesting.2021.107286.

[3] A. Chandra, A. Chandra, R. S. Dhundhel, and A. Bhatt, "Sodium-ion-conducting solid polymer electrolyte: temperature-dependent ionic parameters and solid-state polymer battery fabrication," *Indian J. Phys.*, vol. 96, no. 4, pp. 1069–1074, 2022, doi: 10.1007/s12648-021-02032-1.

[4] Z. Zhang *et al.*, "A mixed electron/ion conducting interlayer enabling ultra-stable cycle performance for solid state lithium sulfur batteries," *J. Power Sources*, vol. 487, no. December 2020, p. 229428, 2021, doi: 10.1016/j.jpowsour.2020.229428.

[5] H. Chen *et al.*, "Functional additives for solid polymer electrolytes in flexible and high-energy-density solid-state lithium-ion batteries," *Carbon Energy*, vol. 3, no. 6, pp. 929–956, 2021, doi: 10.1002/cey2.146.

[6] M. Aparicio, J. Mosa, and A. Durán, "Hybrid organic-inorganic nanostructured membranes for high temperature proton exchange membranes fuel cells (PEMFC)," *J. Sol-Gel Sci. Technol.*, vol. 40, no. 2–3, pp. 309–315, 2006, doi: 10.1007/s10971-006-8370-2.

[7] Y. Daiko, K. Ogura, K. Katagiri, H. Muto, M. Sakai, and A. Matsuda, "Surface-sulfonation and fuel cell properties of phenylsilsesquioxane-based particles," *Solid State Ionics*, vol. 179, no. 21–26, pp. 1166–1169, 2008, doi: 10.1016/j.ssi.2008.02.050.

[8] T. Tezuka, K. Tadanaga, A. Hayashi, and M. Tatsumisago, "Proton-Conductive Inorganic–Organic Hybrid Membrane Prepared from 3-(2-Aminoethylaminopropyl)triethoxysilane and Sulfuric Acid by the Sol-Gel Method," *J. Electrochem. Soc.*, vol. 156, no. 1, p. B174, 2009, doi: 10.1149/1.3023083.

[9] J. Umeda, M. Suzuki, M. Kato, M. Moriya, W. Sakamoto, and T. Yogo, "Proton conductive inorganic-organic hybrid membranes functionalized with phosphonic acid for polymer electrolyte fuel cell," *J. Power Sources*, vol. 195, no. 18, pp. 5882–5888, 2010, doi: 10.1016/j.jpowsour.2009.12.078.

[10] D. R. Vernon, F. Meng, S. F. Dec, D. L. Williamson, J. A. Turner, and A. M. Herring,

"Synthesis, characterization, and conductivity measurements of hybrid membranes containing a mono-lacunary heteropolyacid for PEM fuel cell applications," *J. Power Sources*, vol. 139, no. 1–2, pp. 141–151, 2005, doi: 10.1016/j.jpowsour.2004.07.027 .

[11] H. Kalita, P. Pal, S. Dhara, and A. Pathak, "Fabrication and characterization of polyvinyl alcohol/metal (Ca, Mg, Ti) doped zirconium phosphate nanocomposite films for scaffold-guided tissue engineering application," *Mater. Sci. Eng. C*, vol. 71, pp. 363–371, 2017, doi: 10.1016/j.msec.2016.09.063.

[12] "Complexes of alkali metal ions with poly(ethylene oxide)," vol. 14, p. 1973, 1973.

[13] M. A. Webb, B. M. Savoie, Z. G. Wang, and T. F. Miller, "Chemically Specific Dynamic Bond Percolation Model for Ion Transport in Polymer Electrolytes," *Macromolecules*, vol. 48, no. 19, pp. 7346–7358, 2015, doi: 10.1021/acs.macromol.5b01437.

[14] H. Wu and C. D. Wick, "Computational investigation on the role of plasticizers on ion conductivity in poly(ethylene oxide) LiTFSI Electrolytes," *Macromolecules*, vol. 43, no. 7, pp. 3502–3510, 2010, doi: 10.1021/ma902758w.

[15] P. Duarte *et al.*, "Cellulose-Based Solid Electrolyte Membranes Through Microwave Assisted Regeneration and Application in Electrochromic Displays," *Front. Mater.*, vol. 7, no. August, pp. 1–9, 2020, doi: 10.3389/fmats.2020.00269.

[16] Y. Wu, Y. Li, Y. Wang, Q. Liu, Q. Chen, and M. Chen, "Advances and prospects of PVDF based polymer electrolytes," *J. Energy Chem.*, vol. 64, pp. 62–84, 2022, doi: 10.1016/j.jechem.2021.04.007.

[17] A. K. Arof, S. Amirudin, S. Z. Yusof, and I. M. Noor, "A method based on impedance spectroscopy to determine transport properties of polymer electrolytes," *Phys. Chem. Chem. Phys.*, vol. 16, no. 5, pp. 1856–1867, 2014, doi: 10.1039/c3cp53830c.

[18] M. H. Buraidah, L. P. Teo, S. R. Majid, and A. K. Arof, "Ionic conductivity by correlated barrier hopping in NH4I doped chitosan solid electrolyte," *Phys. B Condens. Matter*, vol. 404, no. 8–11, pp. 1373–1379, 2009, doi: 10.1016/j.physb.2008.12.027.

[19] S. Kurapati, S. S. Gunturi, K. J. Nadella, and H. Erothu, "Novel solid polymer electrolyte based on PMMA:CH3COOLi effect of salt concentration on optical and conductivity studies," *Polym. Bull.*, vol. 76, no. 10, pp. 5463–5481, 2019, doi: 10.1007/s00289-018-2659-5.

[20] K. H. Teoh, C. S. Lim, and S. Ramesh, "Lithium ion conduction in corn starch based solid polymer electrolytes," *Meas. J. Int. Meas. Confed.*, vol. 48, no. 1, pp. 87–95, 2014, doi: 10.1016/j.measurement.2013.10.040.

[21] J. Li *et al.*, "Approaching high performance PVDF-HFP based solid composite electrolytes

with LLTO nanorods for solid-state lithium-ion batteries," *Int. J. Energy Res.*, vol. 45, no. 5, pp. 7663–7674, 2021, doi: 10.1002/er.6347.

[22] A. K. Arof *et al.*, "Quasi solid state dye-sensitized solar cells based on polyvinyl alcohol (PVA) electrolytes containing I-/I3- redox couple," *Opt. Quantum Electron.*, vol. 46, no. 1, pp. 143–154, 2014, doi: 10.1007/s11082-013-9723-z.

[23] P. N. Gupta and K. P. Singh, "SOLID of H , PO , based PVA complex system," vol. 88, pp. 319–323, 1996.

[24] A. J. Polak, S. Petty-weeks, and A. J. Beuhler, "Applications of novel proton-conducting polymers to hydrogen sensing," *Sensors and Actuators*, vol. 9, no. 1, pp. 1–7, 1986, doi: 10.1016/0250-6874(86)80001-4.

[25] I. Der Wu and F. C. Chang, "Determination of the interaction within polyester-based solid polymer electrolyte using FTIR spectroscopy," *Polymer (Guildf).*, vol. 48, no. 4, pp. 989–996, 2007, doi: 10.1016/j.polymer.2006.12.045.

[26] S. Nasri, A. Oueslati, I. Chaabane, and M. Gargouri, "AC conductivity, electric modulus analysis and electrical conduction mechanism of RbFeP2O7 ceramic compound," *Ceram. Int.*, vol. 42, no. 12, pp. 14041–14048, 2016, doi: 10.1016/j.ceramint.2016.06.011.

[27] A. Mohamed Saat and M. R. Johan, "The surface structure and thermal properties of novel polymer composite films based on partially phosphorylated poly(vinyl alcohol) with aluminum phosphate," *Sci. World J.*, vol. 2014, 2014, doi: 10.1155/2014/439839.

[28] V. Koleva and V. Stefov, "Phosphate ion vibrations in dihydrogen phosphate salts of the type M(H 2PO4)2·2H2O (M = Mg, Mn, Co, Ni, Zn, Cd): Spectra-structure correlations," *Vib. Spectrosc.*, vol. 64, pp. 89–100, 2013, doi: 10.1016/j.vibspec.2012.11.004.

[29] C. C. Yang and S. J. Lin, "Preparation of composite alkaline polymer electrolyte," *Mater. Lett.*, vol. 57, no. 4, pp. 873–881, 2002, doi: 10.1016/S0167-577X(02)00888-1.

[30] F. H. Abd El-kader, W. H. Osman, K. H. Mahmoud, and M. A. F. Basha, "Dielectric investigations and ac conductivity of polyvinyl alcohol films doped with europium and terbium chloride," *Phys. B Condens. Matter*, vol. 403, no. 19–20, pp. 3473–3484, 2008, doi: 10.1016/j.physb.2008.05.009.

[31] Z. Yang, H. Peng, W. Wang, and T. Liu, "Crystallization behavior of poly(ε-caprolactone)/layered double hydroxide nanocomposites," *J. Appl. Polym. Sci.*, vol. 116, no. 5, pp. 2658–2667, 2010, doi: 10.1002/app.

[32] G. J. Thangamani, K. Deshmukh, N. A. Nambiraj, and S. K. K. Pasha, "Chemiresistive gas sensors based on vanadium pentoxide reinforced polyvinyl alcohol/polypyrrole blend nanocomposites for room temperature LPG sensing,"

Synth. Met., vol. 273, no. March, 2021, doi: 10.1016/j.synthmet.2020.116687.

[33] H. E. Assender and A. H. Windle, "Crystallinity in poly(vinyl alcohol). 1. An X-ray diffraction study of atactic PVOH," *Polymer (Guildf).*, vol. 39, no. 18, pp. 4295–4302, 1998, doi: 10.1016/S0032-3861(97)10296-8.

[34] A. Mohamed Saat and M. R. Johan, "Effect of phosphoric acid concentration on the optical properties of partially phosphorylated PVA complexes," *Int. J. Polym. Sci.*, vol. 2014, 2014, doi: 10.1155/2014/495875.

[35] L. Li, L. Xu, and Y. Wang, "Novel proton conducting composite membranes for direct methanol fuel cell," *Mater. Lett.*, vol. 57, no. 8, pp. 1406–1410, 2003, doi: 10.1016/S0167-577X(02)00998-9.

[36] L. Yuan *et al.*, "Flexible solid-state supercapacitors based on carbon nanoparticles/MnO 2 nanorods hybrid structure," *ACS Nano*, vol. 6, no. 1, pp. 656–661, 2012, doi: 10.1021/nn2041279.

[37] Z. Osman, M. I. M. Ghazali, L. Othman, and K. B. Isa, "Results in Physics AC ionic conductivity and DC polarization method of lithium ion transport in PMMA – LiBF 4 gel polymer electrolytes," vol. 2, pp. 1–4, 2012, doi: 10.1016/j.rinp.2011.12.001.

[38] M. M. E. Jacob, S. R. S. Prabaharan, and S. Radhakrishna, "Effect of PEO addition on the electrolytic and thermal properties of PVDF-LiClO4 polymer electrolytes," *Solid State Ionics*, vol. 104, no. 3–4, pp. 267–276, 1997, doi: 10.1016/s0167-2738(97)00422-0.

[39] "on Transport in Solvent-Free Polymers," pp. 109–124, 1988.

[40] L. Othman, K. W. Chew, and Z. Osman, "Impedance spectroscopy studies of poly (methyl methacrylate)-lithium salts polymer electrolyte systems," *Ionics (Kiel).*, vol. 13, no. 5, pp. 337–342, 2007, doi: 10.1007/s11581-007-0120-0.

[41] C. S. Ramya, S. Selvasekarapandian, T. Savitha, G. Hirankumar, and P. C. Angelo, "Vibrational and impedance spectroscopic study on PVP-NH4SCN based polymer electrolytes," *Phys. B Condens. Matter*, vol. 393, no. 1–2, pp. 11–17, 2007, doi: 10.1016/j.physb.2006.11.021.

[42] P. Ben Ishai, M. S. Talary, A. Caduff, E. Levy, and Y. Feldman, "Electrode polarization in dielectric measurements: A review," *Meas. Sci. Technol.*, vol. 24, no. 10, 2013, doi: 10.1088/0957-0233/24/10/102001.

[43] S. K. Barik, S. Ahmed, and S. Hajra, "Studies of dielectric relaxation and impedance analysis of new electronic material: (Sb 1/2 Na 1/2)(Fe 2/3 Mo 1/3)O 3," *Appl. Phys. A Mater. Sci. Process.*, vol. 125, no. 3, p. 0, 2019, doi: 10.1007/s00339-019-2496-x.

[44] R. Khalil, "Impedance and

modulus spectroscopy of poly(vinyl alcohol)-Mg[ClO4]2 salt hybrid films," *Appl. Phys. A Mater. Sci. Process.*, vol. 123, no. 6, pp. 1–7, 2017, doi: 10.1007/s00339-017-1026-y.

[45] M. Hema, S. Selvasekerapandian, A. Sakunthala, D. Arunkumar, and H. Nithya, "Structural, vibrational and electrical characterization of PVA-NH4Br polymer electrolyte system," *Phys. B Condens. Matter*, vol. 403, no. 17, pp. 2740–2747, 2008, doi: 10.1016/j.physb.2008.02.001.

[46] S. R. Elliott, "Frequency-dependent conductivity in ionic glasses: A possible model," *Solid State Ionics*, vol. 27, no. 3, pp. 131–149, 1988, doi: 10.1016/0167-2738(88)90003-3.

[47] D. S. McLachlan and G. Sauti, "The AC and DC conductivity of nanocomposites," *J. Nanomater.*, vol. 2007, 2007, doi: 10.1155/2007/30389.

[48] S. T. Senthilkumar, R. K. Selvan, N. Ponpandian, and J. S. Melo, "Redox additive aqueous polymer gel electrolyte for an electric double layer capacitor," *RSC Adv.*, vol. 2, no. 24, pp. 8937–8940, 2012, doi: 10.1039/c2ra21387g.

[49] B.E.Conway, *Electrochemical supercapacitor*, 1st ed. New York: Springer Science+Business Media New York, 1999.

[50] D. Yuan, J. Zeng, N. Kristian, Y. Wang, and X. Wang, "Bi2O3 deposited on highly ordered mesoporous carbon for supercapacitors," *Electrochem. commun.*, vol. 11, no. 2, pp. 313–317, 2009, doi: 10.1016/j.elecom.2008.11.041.

[51] A.K.Jonscher, *Dielectric Relaxation in Solids*. London: Chelsea Dielectric Press, London, 1983.

[52] S. B. Aziz, "Li+ ion conduction mechanism in poly (ε-caprolactone)-based polymer electrolyte," *Iran. Polym. J. (English Ed.*, vol. 22, no. 12, pp. 877–883, 2013, doi: 10.1007/s13726-013-0186-7.

[53] S. B. Aziz, M. A. Brza, S. R. Saed, M. H. Hamsan, and M. F. Z. Kadir, "Ion association as a main shortcoming in polymer blend electrolytes based on CS:PS incorporated with various amounts of ammonium tetrafluoroborate," *J. Mater. Res. Technol.*, vol. 9, no. 3, pp. 5410–5421, 2020, doi: 10.1016/j.jmrt.2020.03.067.

[54] S. B. Aziz and Z. H. Z. Abidin, "Electrical and morphological analysis of chitosan:AgTf solid electrolyte," *Mater. Chem. Phys.*, vol. 144, no. 3, pp. 280–286, 2014, doi: 10.1016/j.matchemphys.2013.12.029.

[55] M. F. Shukur, R. Ithnin, and M. F. Z. Kadir, "Electrical characterization of corn starch-LiOAc electrolytes and application in electrochemical double layer capacitor," *Electrochim. Acta*, vol. 136, pp. 204–216, 2014, doi: 10.1016/j.electacta.2014.05.075.

[56] S. B. Aziz, R. M. Abdullah, M. F. Z. Kadir, and H. M. Ahmed, "Non suitability of silver ion conducting polymer electrolytes

based on chitosan mediated by barium titanate (BaTiO3) for electrochemical device applications," *Electrochim. Acta*, vol. 296, pp. 494–507, 2019, doi: 10.1016/j.electacta.2018.11.081.

[57] S. B. Aziz, "Study of electrical percolation phenomenon from the dielectric and electric modulus analysis," *Bull. Mater. Sci.*, vol. 38, no. 6, pp. 1597–1602, 2015, doi: 10.1007/s12034-015-0978-9.

[58] S. Navaratnam, K. Ramesh, and W. J. Basirun, "Investigation of ion conducting behaviour of composite chitosan based polymer electrolytes," *Mater. Res. Innov.*, vol. 15, no. SUPPL. 2, pp. 3–5, 2011, doi: 10.1179/143307511X13031890748975.

[59] S. B. Aziz, Z. H. Z. Abidin, and A. K. Arof, "Influence of silver ion reduction on electrical modulus parameters of solid polymer electrolyte based on chitosansilver triflate electrolyte membrane," *Express Polym. Lett.*, vol. 4, no. 5, pp. 300–310, 2010, doi: 10.3144/expresspolymlett.2010.38.

[60] A. S. F. M. Asnawi *et al.*, "Glycerolized Li+ ion conducting chitosan-based polymer electrolyte for energy storage EDLC device applications with relatively high energy density," *Polymers (Basel).*, vol. 12, no. 6, pp. 1–19, 2020, doi: 10.3390/polym12061433.

[61] M. F. Shukur, R. Ithnin, H. A. Illias, and M. F. Z. Kadir, "Proton conducting polymer electrolyte based on plasticized chitosan-PEO blend and application in electrochemical devices," *Opt. Mater. (Amst).*, vol. 35, no. 10, pp. 1834–1841, 2013, doi: 10.1016/j.optmat.2013.03.004.

[62] M. Singh, V. K. Singh, K. Surana, B. Bhattacharya, P. K. Singh, and H. W. Rhee, "New polymer electrolyte for electrochemical application," *J. Ind. Eng. Chem.*, vol. 19, no. 3, pp. 819–822, 2013, doi: 10.1016/j.jiec.2012.10.023.

[63] S. B. Aziz, R. B. Marif, M. A. Brza, M. H. Hamsan, and M. F. Z. Kadir, "Employing of Trukhan model to estimate ion transport parameters in PVA based solid polymer electrolyte," *Polymers (Basel).*, vol. 11, no. 10, 2019, doi: 10.3390/polym11101694.

[64] S. B. Aziz *et al.*, "Ion transport study in CS: POZ based polymer membrane electrolytes using Trukhan model," *Int. J. Mol. Sci.*, vol. 20, no. 21, 2019, doi: 10.3390/ijms20215265.

[65] P. A. R. D. Jayathilaka, M. A. K. L. Dissanayake, I. Albinsson, and B. E. Mellander, "Dielectric relaxation, ionic conductivity and thermal studies of the gel polymer electrolyte system PAN/EC/PC/LiTFSI," *Solid State Ionics*, vol. 156, no. 1–2, pp. 179–195, 2003, doi: 10.1016/S0167-2738(02)00616-1.

[66] S. B. Aziz and S. M. Mamand, "The Study of dielectric properties and conductivity relaxation of ion conducting chitosan: NaTf based solid electrolyte," *Int. J. Electrochem.*

Sci., vol. 13, no. 11, pp. 10274–10288, 2018, doi: 10.20964/2018.11.05.

[67] C. G. Koops, "On the dispersion of resistivity and dielectric constant of some semiconductors at audiofrequencies," *Phys. Rev.*, vol. 83, no. 1, pp. 121–124, 1951, doi: 10.1103/PhysRev.83.121.

[68] J. M. Hadi *et al.*, "Electrical, dielectric property and electrochemical performances of plasticized silver ion-conducting chitosan-based polymer nanocomposites," *Membranes (Basel).*, vol. 10, no. 7, pp. 1–22, 2020, doi: 10.3390/membranes10070151.

[69] B. Louati, F. Hlel, and K. Guidara, "Ac electrical properties and dielectric relaxation of the new mixed crystal (Na0.8Ag0.2)2PbP2O7," *J. Alloys Compd.*, vol. 486, no. 1–2, pp. 299–303, 2009, doi: 10.1016/j.jallcom.2009.06.148.

[70] N. H. Idris, H. B. Senin, and A. K. Arof, "Dielectric spectra of LiTFSI-doped chitosan/PEO blends," *Ionics (Kiel).*, vol. 13, no. 4, pp. 213–217, 2007, doi: 10.1007/s11581-007-0093-z.

[71] S. B. Aziz, W. O. Karim, and H. O. Ghareeb, "The deficiency of chitosan: AgNO3 polymer electrolyte incorporated with titanium dioxide filler for device fabrication and membrane separation technology," *J. Mater. Res. Technol.*, vol. 9, no. 3, pp. 4692–4705, 2020, doi: 10.1016/j.jmrt.2020.02.097.

[72] S. B. Aziz, "Role of dielectric constant on ion transport: Reformulated Arrhenius equation," *Adv. Mater. Sci. Eng.*, vol. 2016, 2016, doi: 10.1155/2016/2527013.

[73] R. Richert, "The modulus of dielectric and conductive materials and its modification by high electric fields," *J. Non. Cryst. Solids*, vol. 305, no. 1–3, pp. 29–39, 2002, doi: 10.1016/S0022-3093(02)01085-2.

[74] S. B. Aziz, "Occurrence of electrical percolation threshold and observation of phase transition in chitosan $(1-x)$:AgI x $(0.05 \leq x \leq 0.2)$-based ion-conducting solid polymer composites," *Appl. Phys. A Mater. Sci. Process.*, vol. 122, no. 7, pp. 1–13, 2016, doi: 10.1007/s00339-016-0235-0.

[75] R. Baskaran, S. Selvasekarapandian, N. Kuwata, J. Kawamura, and T. Hattori, "ac impedance, DSC and FT-IR investigations on (x)PVAc-(1 - x)PVdF blends with LiClO4," *Mater. Chem. Phys.*, vol. 98, no. 1, pp. 55–61, 2006, doi: 10.1016/j.matchemphys.2005.08.063.